Chaos, Solitons and Fractals 164 (2022) 112669

Contents lists available at ScienceDirect

Chaos, Solitons and Fractals

journal homepage: www.elsevier.com/locate/chaos

Emergence of Canard induced mixed mode oscillations in a slow–fast dynamics of a biophysical excitable model

Sanjeev Kumar Sharma [a], Arnab Mondal [a], Argha Mondal [b,c,*], M.A. Aziz-Alaoui [d,**], Ranjit Kumar Upadhyay [a], Jun Ma [e]

[a] Department of Mathematics and Computing, Indian Institute of Technology (Indian School of Mines), Dhanbad 826004, India
[b] Department of Mathematics, Sidho-Kanho-Birsha University, Purulia 723104, WB, India
[c] Department of Mathematical Sciences, University of Essex, Wivenhoe Park, UK
[d] Normandie Univ, UNIHAVRE, LMAH, FR-CNRS-3335, ISCN, 76600, Le Havre, France
[e] Department of Physics, Lanzhou University of Technology, Lanzhou 730050, PR China

ARTICLE INFO

Keywords:
FHR model
Slow–fast dynamics
Bifurcation scenarios
Canard phenomenon
MMOs and MMBOs

ABSTRACT

We study the dynamics of a biophysically motivated slow–fast FitzHugh–Rinzel (FHR) model neurons in understanding the complex dynamical behavior of neural computation. We discuss the mathematical frameworks of diverse excitabilities and repetitive firing responses due to the applied stimulus using the slow–fast system. The results focus on the multiple time scale dynamics that include canard phenomenon induced mixed mode oscillations (MMOs) and mixed mode bursting oscillations (MMBOs). The bifurcation structure of the system is examined with injected current stimulus as the relevant parameter. We use the folded node theory to study the canards near the fold points. Further, we demonstrate the homoclinic bifurcation and the transition route to chaos through MMOs. It helps us in understanding the fundamentals of such complex rich neuronal responses. To show the chaotic nature in certain parameter regime, we compute the Lyapunov spectrum as a function of time and predominant parameter, I, that establishes our findings. Finally, we conclude that our observed results may have major significance and discuss the potential applications of MMOs in neural dynamics.

1. Introduction

This article presents a detailed discussion of a slow–fast dynamical model neuron [1–4] and its characteristics that generally exhibits elliptic bursting. It introduces the mechanism of generating complex oscillations in a biophysical system of coupled nonlinear ODEs with slow–fast time scales. We consider one predominant parameter in the system and when it moves slowly, the spike transitions occur. Some neuronal systems exhibit spontaneous firing activity with multiple timescale dynamics, in particular called bursting that consists of periods of repetitive firing interspersed by quiescent/silent phases. During the active phases, it eventually shows a burst, recovers slowly during the silent phase, and the system prepares to initiate the next burst of spikes [5,6]. The underlying mechanism of information processing in the neural system depends on the cellular membrane voltages, when it reaches certain values above threshold, it exhibits spiking–bursting oscillations by varying injected stimuli. Such oscillatory dynamics of membrane voltage can be mathematically modeled using various dynamical systems of coupled ODEs (with different realistic parameters) [7–9].

One of the most interesting complex dynamical oscillations that emerge from the electrical activity of neurons is the mixed-mode oscillations (MMOs) [10–15]. MMOs are used to describe the alternating trajectories that is a combination of small and large amplitude oscillations (SAOs and LAOs). MMOs present complex periodic waveforms in which each period is comprised of different maxima and minima of various amplitudes. Recently, researchers have been showing a great interest in the theory of MMOs with canard solutions [16–20]. Such MMOs arise in the slow–fast dynamics. The neuron receives a constant input current and produces rich firing patterns that can represent the system dynamics regarding the neuronal responses. Using stability analysis and bifurcation theory, we find the rich firings with MMOs/MMBOs that can be induced by canard phenomenon. MMBOs: there arises small amplitude slow oscillations i.e., SAOs and LAOs sometimes consist of bursts. MMOs and MMBOs [21] may be periodic or aperiodic in nature. These make the model fascinating and the results provide interesting and potential applications in this type of slow–fast biophysically plausible system. In MMBOs, the firing patterns consist

* Corresponding author at: Department of Mathematical Sciences, University of Essex, Wivenhoe Park, UK.
** Corresponding author.
E-mail addresses: arghamondalb1@gmail.com (A. Mondal), aziz.alaoui@univ-lehavre.fr (M.A. Aziz-Alaoui).

https://doi.org/10.1016/j.chaos.2022.112669
Received 22 June 2022; Accepted 4 September 2022
Available online 27 September 2022

of SAOs and LAOs together with bursting in the LAOs. The emergence of MMBOs in the system creates a spike adding mechanism.

The emergence of SAOs during the occurrence of the trajectories near a fold point is generated in the presence of folded singularity. To understand the mechanisms of MMOs, we have to study the flow near the folded singularities and the special solutions are canard phenomenon. The *canard* term was first introduced to show the periodic solutions in the Van der Pol equation that stay near the repelling slow manifold [22]. The major part of canard cycles is that it exists for an exponentially small region of parameters. This transition phase is called canard explosion [12,18,23,24]. The canard solutions are derived that connect the attracting slow manifold with repelling slow manifold. In dynamical systems with one or more than one slow variable, canard emerges in a robust fashion with SAOs close to the folded singularity [25–28]. Our slow–fast system has the critical manifold with cubic curve. Bursting arises through a supercritical Hopf bifurcation followed by a canard explosion with MMOs and MMBOs induced in the system.

In previous studies, it was observed that the MMOs reflect the dynamical and neuronal behavior of locomotion or breathing [29]. The multiple time scale dynamics and noise can also induce MMOs [30,31]. It was found in calcium signaling and electrocardiac systems [32–34]. We find that, the generation of MMOs can be analyzed by using the canard phenomenon from dynamical system approaches [25,29]. Krupa et al. [35] examined the mechanism of MMOs oscillations in a two-compartmental model of dopaminergic neurons in the mammalian brain stem. Previously, it was investigated the generation of MMOs in a coupled FitzHugh–Nagumo (FHN) model [27,36]. MMOs can also generate a type of bursting that can be reflected in a biophysical model of pituitary lactotroph [37] and it was also observed in stellate cells of the medial entorhinal cortex (layer II), the mechanism of such patterns was analyzed in a conductance-based model [26]. Recently, it has been investigated how the changes in the conductance of the voltage-gated calcium channels as well as the parameter corresponding to the fraction of free cytosolic calcium concentration in an excitable model affect the neuronal behavior leading to transition from pseudo-plateau bursting to MMOs [38]. Bertram et al.'s work [39] showed that the model of pancreatic β-cells can also exhibit MMOs and MMBOs. Apart from these works including single and coupled biophysical models, researchers investigate the firing activities and collective patterns in a neural network, where neurons are connected in a complex network structure [40–42]. MMOs were observed in pre-Botzinger complex networks (a medullary region that controls breathing in mammals) [13]. Currently, we explored the emergence of tonic spiking and MMOs in a random network of diffusively coupled Izhikevich neurons in a backdrop of diverse excitabilities [43].

In this study, it has been demonstrated the dynamics of a solitary nerve membrane using the suitable FHR model [2–4], that is the modification of the classical two dimensional (2D) FHN model. We explain how the system dynamics differ from the FHN model [5]. It exhibits interesting properties that are relevant to biophysical excitabilities and spike generation. However, the model cannot generate various rich firing patterns especially found in cortical type neurons [44]. The relation between spiking and bursting shows a significant phenomenon as well as a fascinating neuronal responses, especially in neural coding. The third variable allows to induce a recurrent crossing through the Hopf Bifurcation and it induces bursting oscillations. The first variable, v depends on the two other variables. The transition phases depend on the dynamics of the slow variable and strength of the slowly changing current stimulus. It can produce self organized different firing features for some specified fixed range of parameters. The mathematical model is examined theoretically and numerically. The different parameter sets corresponding to the qualitatively various dynamical properties are analyzed. An interesting feature of the elliptic bursting is that the frequency of emerging spiking activity and ceasing the spiking is nonzero, at that time the amplitude of the oscillations may be small [3,4]. It was experimentally observed that this type of bursting can be found in trifacial nerves controlling the jaw movement of rodents [45,46]. Further, the model neuron exhibiting diverse oscillations can represent large networks of distinct clusters. Recently, Xie et al. [47] studied the dynamics of double mixed mode and double canards numerically for the FHR model. They have used the blowup method to analyze the desingularised system. Here, we use the geometric singular perturbation theory (GSPT) [12] to study the FHR model. We show various types of MMOs and MMBOs, that are not deeply investigated earlier. This study can be useful as a starting point to investigate general neural network structures using slow–fast models. We find the basin of different firing/quiescent regions depending on parameter sets. The model can produce quiescent or oscillatory behavior that can be captured by real neurons. The three dimensional (3D) model represents an interesting classic example of slow–fast dynamics [27,35,42] and under certain conditions on the control parameters, it exhibits canard phenomenon, that shows the solutions which pass from a stable manifold to an unstable manifold for long time range in the slow system timescale [36] and it is verified by Shilnikov bifurcation theory [48,49]. Here, we report how the emergence of MMOs/MMBOs and this oscillations are different from other firings with relevant biophysical significances [50].

The paper is organized as follows: In Section 2, we briefly describe the dynamics of the excitable model equations that shows the electrical potential called as spikes and some basic preliminaries. In Section 3, we demonstrate the canard solution near the fold points using folded node theory with numerical results. Then in Section 4, we discuss the occurrence of Shilnikov type chaos in the system. Further, we report our main findings in Section 5 where the temporal evolution of the FHR model are elaborately discussed with performing the bifurcation results. Finally, we conclude with a discussion in Section 6.

2. Formulation of the excitable model dynamics and some preliminaries

The article focuses on the complex dynamics of the excitable FHR system that describes the electrical activities of neural membrane voltage over an appropriate range of parameter values. The model is computationally efficient to analyze widely meaningful dynamically rich properties. The time evolution of such a mathematical model is described by the following set of ODEs [2–4]

$$\begin{aligned}\frac{dv}{dt} &= v - v^3/3 - w + y + I = f(v,w,y),\\ \frac{dw}{dt} &= \delta(a + v - bw) = g_1(v,w,y),\\ \frac{dy}{dt} &= \mu(c - v - dy) = g_2(v,w,y),\end{aligned} \tag{1}$$

where v, w and y represent the membrane voltage, recovery variable and slow modulation of the current respectively. The parameter, I measures constant external injected current and a, b, c, d, δ and μ are the system parameters. δ and μ indicate small parameters that determine the pace of the slow system variables, w and y respectively. The small parameter μ ranges in $0 < \mu \ll 1$ and we consider $\mu = \delta^2$ [35,51,52] to make the system with three distinct time scales i.e., a fast scale with two slow subscales. We assume $b > 0$ [53], a small parameter. The parameter a in the 2D FHN model corresponds to the parameter value c of the FHR model [3]. If we decrease the value of a, it causes longer intervals between two bursting however, there exists relatively fixed time of bursting duration. With the increase of a, the interburst intervals become shorter and periodic bursting changes to tonic spiking. The model is described by the slow–fast subsystems, the first two equations represent the classical slow–fast FHN model [27,36,42] that generates only spiking. The variable y indicates 'superslow' variable. Particularly, it produces elliptic bursting for a certain fixed set of parameters with large amplitude spikes and small amplitude oscillations [3,4]. It generates decay and growth of small amplitude oscillations during the silent phase of bursting and not damped rapidly.

2.1. Slow–fast dynamical phenomenon in the system

First, we assume the neuron is the onset of firing and it shows spike generation as the control parameter moves slowly. We provide some basic definitions of canard and MMOs, that are observed in our numerical results at the transition of oscillatory patterns. The slow–fast system can be mathematically modeled as [5]

$$\begin{aligned} \dot{x}(t) &= f(x,\ z), \\ \dot{z}(t) &= \delta g(x,\ z), \end{aligned} \tag{2}$$

where $\dot{x}(t) = f(x,\ z)$ (fast spiking) and $\dot{z}(t) = \delta g(x,\ z)$ (slow modulation). $x \in \mathbb{R}^m$ represents the fast variables and $z \in \mathbb{R}^n$ the slow variables with $0 < \delta << 1$ measure the timescale separation parameter. In this dynamics, the singular limit corresponding to $\delta = 0$ is called the layer system and then z, the slow variable presents a parameter in the limiting system [35,36,54,55].

Definition 2.1.1. For a slow–fast dynamical system, with the timescale separable parameter $\delta = 0$,
$C = \{(x,\ z) \in \mathbb{R}^m \times \mathbb{R}^n :\ f(x,\ z) = 0\}$ is defined as the critical manifold and it corresponds to the fixed points of the layer system.

Definition 2.1.2. A subset $C_1 \subset C$, the critical manifold is called normally hyperbolic if all the fixed points in C_1 show hyperbolicity condition of the layer system, i.e., $D_x f$ has no eigenvalues with zero real parts. Dynamically, C_1 is called attracting (or repelling) if the eigenvalues have negative (or positive) real part and C_1 represents a saddle if it neither attracting nor repelling.

Definition 2.1.3 ([36,55])**.** Suppose the set of points in C, that are not hyperbolic points i.e., $D_x f$ has at least one eigenvalue with zero real part as follows

$$C_2 = \left\{ (x,\ z) \in C :\ \begin{array}{c} rank(D_x f(x,\ z)) = m-1, \\ l D_x^2 f(x,\ z)(r,r) \neq 0, \\ l D_z f(x,\ z) \neq 0, \end{array} \right\}$$ where l and r denote left and right eigendirections of $D_x f$. C_2 shows the fold points of the critical manifold C. C_2 locally divides the critical manifold C into subsets of various stabilities.

Definition 2.1.4. A solution of the slow–fast system $\dot{x}(t) = f(x,\ z)$ $\dot{z}(t) = \delta g(x,\ z)$ is called a canard if it stays within $\theta(\delta)$ of a repelling branch of the critical manifold for a time i.e., $\theta(1)$ on the slow timescale dynamics $\tau = \delta t$.

This article is to show the existence of canard induced MMOs/MMBOs in the slow–fast system. We investigate how the fixed points and the fold points of the slow–fast dynamics play major role in the existence of MMOs and Canard. To illustrate this, we study the dynamics of the slow system on the critical manifold. The equilibrium points of the slow–fast system range within a $\theta(\delta)$ neighborhood of the equilibrium points of the reduced system [12,55]. We have to investigate the desingularized system, that can be obtained from the slow dynamics using a particular time scaling. The equilibrium points of the desingularized system rest within an $\theta(\delta)$ neighborhood around the fixed points of the slow–fast system and the fold points. To change the new timescale domain by using $\tau = \delta t$, we obtain the slow–fast dynamics as follows

$$\begin{aligned} \delta \dot{x}(\tau) &= f(x,\ z), \\ \dot{z}(\tau) &= g(x,\ z). \end{aligned} \tag{3}$$

The singular limit corresponding to $\delta = 0$ is called reduced system that represents the differential algebraic equations (DAEs) [21,51] corresponding to slow subsystem $\dot{z}(\tau) = g(x,\ z)$ that is defined on the critical manifold, C. The complete system and the reduced dynamics have the same fixed points. To deduce the desingularized system [54,55], we differentiate $f(x,z) = 0$ from Eq. (3) with respect to τ to obtain the following equation

$$(D_x f).\frac{dx}{d\tau} + (D_z f).\frac{dz}{d\tau} = 0. \tag{4}$$

Now, multiplying both sides of Eq. (4) by $\mathrm{adj}(D_x f)$, the transpose of the cofactor matrix of $D_x f$ can be obtained as follows

$$-\det(D_x f).\frac{dx}{d\tau} = \mathrm{adj}(D_x f).(D_z f).g(x,z), \tag{5}$$

where $\det(D_x f) = 0$ represents the singular system, called fold points. The standard existence uniqueness results do not hold at the fold points. The desingularized system is obtained as follows

$$\begin{aligned} \frac{dx}{d\tau} &= \mathrm{adj}(D_x f).(D_z f).g(x,z), \\ \frac{dz}{d\tau} &= -\det(D_x f).g(x,z). \end{aligned} \tag{6}$$

In the case $m = 1$, $D_x f = \det(D_x f) = \frac{\partial f}{\partial x}$ is a scalar and $\mathrm{adj}(D_x f) = 1$. To obtain the phase space flows of the reduced dynamics from the desingularized system (depending on the new time scale $d\tau = -\det(D_x f)d\tau$), the direction of the flows of the desingularized dynamics must be reversed on the new branches where $\det(D_x f) > 0$. Now, the extended system (6) contains two types of fixed points, that are known as ordinary and folded singularities respectively and we define them as follows

Definition 2.1.5 ([36,55])**.** An equilibrium point of the desingularized system (6) is called as ordinary singularity if the fixed point corresponds to a fixed point of the reduced system and ranges in a neighborhood $(\theta(\delta))$ of an equilibrium point of the complete dynamics. The conditions of the singularity are stated as

$$g(x,z) = 0,\ \det(D_x f) \neq 0,\ \mathrm{adj}(D_x f)(D_z f).g(x,z) \neq 0.$$

Definition 2.1.6 ([36,55])**.** An equilibrium point of the desingularized system is called folded singularity if it corresponds to a folded point of the reduced system. The conditions for a folded singularity are stated as

$$\det(D_x f) = 0, \mathrm{adj}(D_x f)(D_z f).g(x,z) = 0.$$

3. Slow–fast dynamics with canard mechanism

In this section, we first derive the layer system corresponding to Eq. (1) that follows the fast slow dynamics (2). In our case, $x \equiv v$, the fast subsystem and $z \equiv (w,\ y)$ is a two tuple vectors, i.e., it represents that the slow subsystem is two dimensional. The system (1) has two different time scales δ and δ^2 for slow (w) and superslow (y) variables respectively. The layer system is obtained by taking the singular limit $\delta = 0$ in the system (1), where the slow variables (w and y) are treated as a parameter of the singular system (7). The layer system is described by the following set of ODEs

$$\begin{aligned} \frac{dv}{dt} &= v - v^3/3 - w + y + I = f\,(v,w,y)\,, \\ \frac{dw}{dt} &= 0, \\ \frac{dy}{dt} &= 0. \end{aligned} \tag{7}$$

Now, changing the system (1) to the slow time scale $\tau_1 = \delta t$, we obtain $d\tau_1 = \delta dt$. The system (1) reduces to

$$\begin{aligned} \delta \frac{dv}{d\tau_1} &= v - v^3/3 - w + y + I = f\,(v,w,y)\,, \\ \frac{dw}{d\tau_1} &= (a + v - bw)\,, \\ \frac{dy}{d\tau_1} &= \delta\,(c - v - dy)\,, \end{aligned} \tag{8}$$

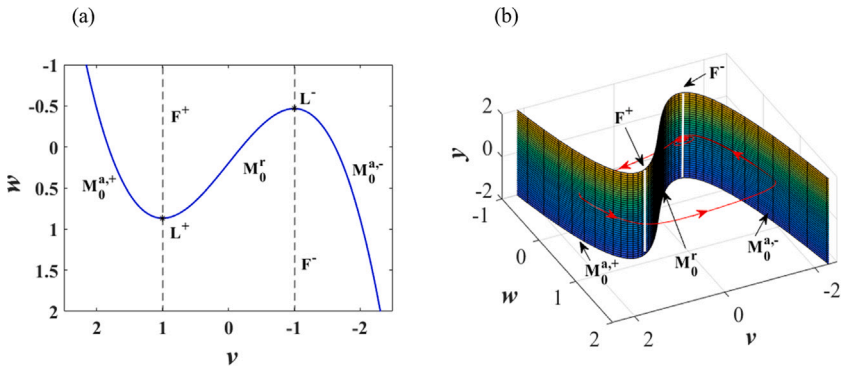

Fig. 1. (a) Critical manifold curve (M_0) of the FHR model with fixed base parameters and $I = 0.21$. (b) Surface plot of the critical manifold (M_0) with relaxation limit cycle with the same parameters as mentioned in Fig. 1(a).

corresponding reduced system is obtained by setting $\delta = 0$ in system (8). Thus, the reduced system can be written as

$$\begin{aligned} 0 &= v - v^3/3 - w + y + I = f(v, w, y), \\ \frac{dw}{d\tau_1} &= (a + v - bw), \\ \frac{dy}{d\tau_1} &= 0. \end{aligned} \tag{9}$$

It is also known as DAEs. The main purpose of studying the GSPT is to understand the dynamics of the full system (1) using subsystems (7) and (9) for $\delta > 0$. The algebraic equation of the above system describes the dynamics of critical manifold (M_0) which can be expressed as follows

$$\begin{aligned} M_0 &= \{(v, w, y) : f(v, w, y) = 0\}, \\ &= \left\{(v, w, y) : v - \frac{v^3}{3} - w + y + I = 0\right\}, \\ &= \left\{(v, w, y) : w = v - \frac{v^3}{3} + y + I\right\}. \end{aligned} \tag{10}$$

The critical manifold is described by a cubic function of v and the shape of the manifold M_0 is similar to the shape of the cubic function (see Fig. 1(a)). It also gives the set of equilibrium points for the layer system (7). From Eq. (9), we obtain $\frac{dy}{d\tau_1} = 0$ therefore, the variable y in M_0 is treated as a constant. The points where M_0 loses its normal hyperbolicity is known as the fold points $(L^{\pm})$. Hence, $L^{\pm}$ decomposes M_0 into three branches, $M_0 = M_0^{a,-} \cup L^- \cup M_0^r \cup L^+ \cup M_0^{a,+}$, where $M_0^{a,-}$ and $M_0^{a,+}$ are the attracting branches of M_0 and is given by $M_0^{a,-} \cup M_0^{a,+} = \left\{(v, w, y) \in M_0 : \frac{\partial f}{\partial v} < 0\right\} = \{(v, w, y) \in M_0 : v < -1 \text{ and } v > 1\}$. M_0^r is the repelling branch of M_0 and it is given by $M_0^r = \left\{(v, w, y) \in M_0 : \frac{\partial f}{\partial v} > 0\right\} = \{(v, w, y) \in M_0 : -1 < v < 1\}$. The black dotted lines in Fig. 1(a) denote the fold lines (F^+ and F^-) of the FHR system. For better visualization, we also draw the manifold (M_0) in a three dimensional (v, w, y) space with a trajectory (see Fig. 1(b)). The left and right fold lines are F^+ and F^- respectively. The right side of F^- and left side of F^+ are the attracting sheets of M_0. The trajectories can reach the fold line F^+ at a jump point (L^+) and follows the fast flow to reach the attracting sheet $M_0^{a,-}$. Now, the trajectories move upward on the attracting sheet towards the fold line F^- and again it jumps from the fold point (L^-) to the attracting sheet $M_0^{a,+}$. We can denote this process by $L^+ \to M_0^{a,-} \to L^- \to M_0^{a,+}$. The points L^- and L^+ are the folds points of M_0 (see Fig. 1(a)) and obtained by satisfying the three conditions mentioned in the definition of fold points. Now, these conditions reduce to $\frac{\partial f}{\partial v}|_{L^{\pm}} = 0$, $\frac{\partial^2 f}{\partial v^2}|_{L^{\pm}} \neq 0$ and $D_{(w,y)} f|_{L^{\pm}}$ has full rank one for one fast and two slow subsystems [12]. From the first condition $\frac{\partial f}{\partial v}|_{L^{\pm}} = 0$, we obtain $1 - v^2 = 0$ i.e., $v = \pm 1$ as fold points of the system (1) and from remaining conditions, we obtain $\frac{\partial^2 f}{\partial v^2}|_{L^{\pm}} = -2$ or 2 and $D_{(w,y)} f|_{L^{\pm}} = (-1, 1)$ with full rank one respectively.

Now, to describe the slow flow in terms of the fast variable v, we differentiate the algebraic equations $f(v, w, y) = 0$ with respect to τ_1, which gives $\frac{df}{dv}\frac{dv}{d\tau_1} + \frac{df}{dw}\frac{dw}{d\tau_1} + \frac{df}{dy}\frac{dy}{d\tau_1} = 0$ or $\left(1 - v^2\right)\frac{dv}{d\tau_1} - \frac{dw}{d\tau_1} = 0$. Substituting the value of $\frac{dw}{d\tau_1}$ from (9), we obtain

$$-\left(1 - v^2\right)\frac{dv}{d\tau_1} = -\left(a + v - b\left(v - \frac{v^3}{3} + y + I\right)\right).$$

Generally, one can append a slow subsystem to the above equation to make it a slow–fast system. The resulting two-dimensional system is singular on the fold curve. We can desingularize the slow flow near the fold points $v^* = \pm 1$ by rescaling the time domain as $d\tau_1 = -\left(1 - v^2\right)d\tau_2$. Therefore, we obtain the desingularized reduced system (DRS) expressed as [51]

$$\begin{aligned} \frac{dv}{d\tau_2} &= -\left(a + (1 - b)v - b\left(-\frac{v^3}{3} + y + I\right)\right), \\ \frac{dy}{d\tau_2} &= -\delta\left(1 - v^2\right)(c - v - dy), \end{aligned} \tag{11}$$

restricted to M_0. The folded singularity can be classified as folded saddle, folded node or folded focus depending on the nature of the eigenvalues of the Jacobian matrix of the DRS at the folded singularity. We obtain the folded singularities as equilibrium of the system (11) which lie on the fold lines $F^{\pm}$. The DRS system (11) has two types of singularities, one is folded singularity and other is ordinary singularity. The unique equilibrium that stays on the fold line F^+ is $v^* = 1, y^* = \frac{1}{b}(a + 1(-2 - 3I)b)$ with $w = \frac{a+1}{b}$. Similarly, the only equilibrium point that lies on the fold line F^- is $v^* = -1, y^* = \frac{1}{b}(a - 1(2 - 3I)b)$ with $w = \frac{a-1}{b}$. These two equilibrium points are known as folded singularities of the DRS system (11). The ordinary equilibrium point is obtained by solving the equations $c - v - dy = 0$ and $\left(a + (1 - b)v - b\left(-\frac{v^3}{3} + y + I\right)\right) = 0$ for v and y respectively. The Jacobian matrix of the DRS around the folded singularity is given by

$$J_{DRS} = \begin{pmatrix} -1 & b \\ 2\delta v^*(c - v^* - dy^*) & 0 \end{pmatrix}.$$

Now, we consider ξ_1 and ξ_2 be the eigenvalues of J_{DRS} at the point (v^*, y^*) restricted to M_0. Then, we classify the point (v^*, y^*) depending on the folded singularities as follows

$$\begin{cases} \text{folded node} & \text{if } \xi_1\xi_2 > 0,\ \xi_{1,2} \in \mathbb{R}, \\ \text{folded focus} & \text{if } \xi_1\xi_2 > 0,\ \mathrm{Im}(\xi_{1,2}) \neq 0, \end{cases}$$

Generally, the folded node and folded saddle–node equilibria can be observed in a system which exhibits mixed-mode dynamics [35]. Here, we will explore different dynamics of MMOs and MMBOs in the case of folded node.

Remark 1 ([12]). For the slow–fast system (1) with $\delta > 0$ sufficiently small, the following conditions hold

(a) Consider $\psi = \frac{\xi_w}{\xi_s} < 1$ for a folded node, then the singular canard $\widetilde{\gamma}_s$ ("the strong canard") always perturbs to a maximal canard γ_s. If $\psi^{-1} \notin \mathbb{N}$, then the singular canard $\widetilde{\gamma}_w$ ("the weak canard")

also perturbs to a maximal canard γ_w, where γ_s and γ_w denote primary canards. For a folded node, suppose $n > 0$ is an integer such that $2n+1 < \psi^{-1} < 2n+3$ and $\psi^{-1} \neq (2n+2)$. Then, in addition to $\gamma_{s,w}$, there are at most n other maximal canards, that are indicated as secondary canards.

(b) For a folded focus, there are no maximal canards.

4. Shilnikov type chaos

Homoclinic bifurcation unfolds many fundamental stretching and foldings of chaos. We show the evidences of MMOs as a transition route to the homoclinic chaos. In this section, we have analytically derived the condition for the existence of one real and two complex conjugate roots in the system (1).

Proposition 4.1. *There exists a unique real equilibrium state for the FHR model (1) that contains one real and two complex conjugate eigenvalues for negative discriminant of the characteristic polynomial.*

Proof. The equilibrium points of the system (1) are derived as $w^* = (v^* + a)/b$, $y^* = (c - v^*)/d$ and $v^{*3} - 3v^*r = s$, where $r = \left(1 - \frac{1}{b} - \frac{1}{d}\right)$ and $s = \left(3I - \frac{3a}{b} + \frac{3c}{d}\right)$ respectively. Depending on the nature of discriminant of the cubic equation $v^{*3} - 3v^*r - s = 0$, the system (1) can have maximum three equilibrium states. The discriminant of the above cubic polynomial is given by $-\left[4(\frac{3}{b})^3 + 27(3c + \frac{3a}{b} - 3I)^2\right] < 0$ for $b > 0$ and $d = 1$, which indicates that there exists a unique real equilibrium state. By solving the above cubic equation, we obtain $v^* = \frac{3\sqrt[3]{2}}{A} - \frac{A}{3\sqrt[3]{2}b}$, where $A = \sqrt[3]{81ab^2 + \sqrt{\left(81ab^2 - 81b^3c - 81b^3I\right)^2 + 2916b^3}} - 81b^3c - 81b^3I$. Now, we can linearize the system (1) around the unique equilibrium point (v^*, w^*, y^*) to obtain the variational matrix (J) given by

$$J\left(v^*\right) = \begin{pmatrix} 1 - v^{*2} & -1 & 1 \\ \delta & -\delta b & 0 \\ -\delta^2 & 0 & -\delta^2 \end{pmatrix}.$$

The characteristic polynomial of the matrix J is given by $P(\eta) = \eta^3 - \left(1 - v^{*2} - \delta b - \delta^2\right)\eta^2 + \left(\delta - \delta b + b\delta^2 + b\delta v^{*2} + \delta^2 v^{*2}\right)\eta - \left(-\delta^3 - b\delta^3 v^{*2}\right)$.

The determinant of the matrix J is obtained as $\det(J) = -\delta^3(1 + bv^{*2}) < 0$, which indicates that at least one root of $P(\eta)$ is negative. To find the nature of the roots of the characteristic polynomial, we evaluate the discriminant, D of the above cubic polynomial, $P(\eta)$, which is given by

$$\begin{aligned} D = {} & 18\left(b\delta^3 - b\delta + b\delta v^{*2} + \delta + \delta^2 v^{*2}\right)\left(b\delta^3 v^{*2} + \delta^3\right)\left(b\delta + \delta^2 + v^{*2} - 1\right) \\ & - 4\left(b\delta^3 v^{*2} + \delta^3\right)\left(b\delta + \delta^2 + v^{*2} - 1\right)^3 \\ & + \left(b\delta^3 - b\delta + b\delta v^{*2} + \delta + \delta^2 v^{*2}\right)^2\left(b\delta + \delta^2 + v^{*2} - 1\right)^2 \\ & - 4\left(b\delta^3 - b\delta + b\delta v^{*2} + \delta + \delta^2 v^{*2}\right)^3 - 27\left(b\delta^3 v^{*2} + \delta^3\right)^2. \end{aligned}$$

If $D < 0$, then $P(\eta)$ has one real and a pair of complex conjugate roots $(\sigma, \eta_1 \pm i\eta_2)$ whereas for $D > 0$, $P(\eta)$ has three real roots. Here, we are only interested in finding the value of the parameters for which $D < 0$.

Definition 4.1. The equilibrium point of the 3D system (1) is called a hyperbolic saddle focus if the eigenvalues of J, evaluated at the same equilibrium point, are $\lambda_1 = \sigma$ and $\lambda_{2,3} = \eta_1 \pm i\eta_2$, where $\sigma\eta_1 < 0$ and $\eta_2 \neq 0$.

Proposition 4.2 ([48,49,56]). *The Shilnikov-type homoclinic chaos exists in a 3D system having saddle focus equilibrium point in a 3D continuous autonomous dynamical system. Consider the eigenvalues of the system as $\lambda_1 = \sigma$ and $\lambda_{2,3} = \eta_1 \pm i\eta_2$, then the occurrence of the Shilnikov chaos deal with the conditions $\sigma < 0$ and $\eta_1 > 0$ or $\sigma > 0$ and $\eta_1 < 0$ with $|\frac{\sigma}{\eta_1}| > 1$, where the trajectories in the two dimensional eigenspace evolve spirally outward from a saddle focus equilibrium and insert into it again along the stable eigendirection with $\sigma < 0$ and $\eta_1 > 0$.*

Now, we define the saddle value as $\sigma_1 = \sigma + \eta_1$ and saddle index as $\nu = |\frac{\eta_1}{\sigma}|$. The dynamics of the system (1) near the saddle focus is simple for $\sigma_1 < 0$ or $\nu < 1$ and complex for $\sigma_1 > 0$ or $\nu > 1$ [49]. In this study, we restrict our findings on the simpler condition $|\frac{\sigma}{\eta_1}| > 1$ for the occurrence of Shilnikov chaos when we discuss the sequences of MMOs and MMBOs with the transition route to homoclinic bifurcation and associated firings in the slow–fast biophysical system.

The parameter sets for all the simulation results are considered as $a = 0.7$, $\delta = 0.08$, $b = 0.8$, $c = -0.775$, $d = 1$ with varying I [3,4]. In order to study the system dynamics, we first analyze the equilibrium states and then bifurcations. The numerical simulations of the systems of ODEs are performed using the fourth-order Runge–Kutta method with a long time span ($t = 100000$) and more than that using the time step $\Delta t = 0.01$. The simulation results with a smaller time step do not show any significant differences. Bifurcation diagram of the fixed points of the dynamical model is computed using the MatCont software package [57].

5. Results

In this article, we present the dynamics of MMOs and MMBOs, it creates a spike adding mechanism in the SAOs and as well as in LAOs and how these SAOs are controlled using the folded node theory. Here, the model neuron has been considered as a simple mathematical framework for a single cell dynamics. The model mechanism has a strong sensitivity of the neuronal responses by varying relevant parameters. We provide a description of a sensitive parameter slow–fast where the system changes its firing patterns and firing frequency from quiescent to oscillatory state. To explore the mechanism of the MMOs and MMBOs, we study the reduced system of the FHR model. The DRS system is described by system (11) and corresponding Jacobian matrix is given by J_{DRS}. In this section, we analyze the transition of the dynamics from stable equilibrium solution (quiescent state) to oscillations (bursting, MMOs, MMBOs, tonic spiking) for a range of fixed values of I. The interval is centered around the values of I, where canard solution is occurred.

5.1. Bifurcation analysis

The bifurcation analysis of the system (1) is presented by considering injected current stimulus, I as a predominant parameter. The system has a real fixed point for I, that ranges in a certain fixed interval. The solid and dotted black lines in (Fig. 2(a)) indicate stable and unstable equilibrium branches respectively. At lower current stimulus ($I < 0.13371$), the system has one stable equilibrium branch (stable focus node). There exists a supercritical Hopf bifurcation (HB1) at $I = 0.13371$ and small amplitude stable limit cycle emerges, where the system exhibits subthreshold oscillations. Now, the steady state vanishes and a periodic limit cycle attractor exists in a saddle focus regime for $0.13371 < I < 3.166224$. The system has another stable focus node at higher current stimulus ($3.166224 < I < 3.9435$) and stable node for $I > 3.9435$. An interesting feature arises in the system i.e., multiple switching between the stable (solid green lines) and unstable limit cycle (dotted magenta lines) can be observed. Again, an unstable fixed point with stable limit cycle appears and the system (1) shows second supercritical Hopf bifurcation (HB2) at $I = 3.166224$. In the saddle focus zone, the neuron which was in steady state now becomes excited and shows different types of periodic and aperiodic oscillatory behavior. First it exhibits various types of MMOs, MMBOs and then it shows tonic spiking. Interestingly, as we further increase the strength of I, a different MMOs pattern appear around the HB2 point and then the

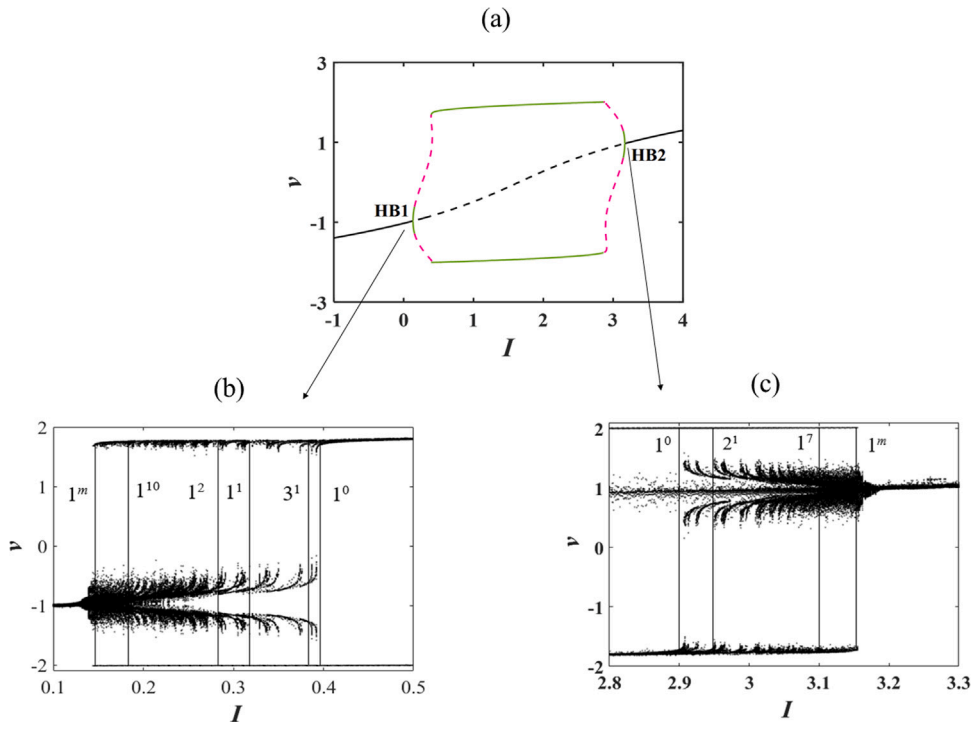

Fig. 2. Bifurcation scenarios of the FHR model (1) with the fixed parameters. (a) Stability of the equilibrium branches and limit cycles. The points HB1 and HB2 denote the supercritical Hopf bifurcations. (b)–(c) Bifurcation diagrams describing the maximum and minimum variations in membrane voltage (v) with I in the neighborhood of HB1 and HB2 respectively. The upper branch represents the peak of the spikes generated in the system (1) whereas the lower branch represents the peak of hyperpolarization. The dark patches around $v = \pm 1$ represent the SAOs in the system (1). (For interpretation of the references to color in this figure legend, the reader is referred to the web version of this article.)

system again converges to quiescent state. The maximum and minimum variations of v with respect to I are shown in Fig. 2(b)–(c). At $I = 0.134$, the steady state enters into an unstable region where the system (1) shows different oscillations. The dark region with branches around $v = \pm 1$ denotes the SAOs with different numbers and amplitudes emerging in the system (1). One interesting phenomenon is observed here that as we slowly increase the value of I, the density of dark region around $v = -1$ decreases. Thus, this indicates that the number of SAOs decreases in the system and there is a transition in firing patterns (see Fig. 3). A similar phenomenon is observed around $v = 1$ however, with decreasing value of I (see Fig. 2(c)).

5.2. Diverse oscillatory responses and route to chaos

The detailed description of the firing transitions, from quiescent state to limit cycle zone is examined as follows. The observed MMOs/MMBOs consist of s number of SAOs with l number of LAOs, i.e., spikes. Around $I = 0.15$, the system exhibits MMOs from the quiescent state ($I = 0.1$, see Fig. 3(a)). It consists of finitely many SAOs of different amplitudes of slow oscillations with single spike in LAOs. It takes the form as $l^s l^s l^s \ldots = 1^m 1^m 1^m \ldots$, where $s = m$, a positive finite integer (see Fig. 3(b)). A similar type of MMOs is also observed at $I = 0.155$ (see Fig. 3(c)). As we increase I, the number of SAOs decreases and the periodic nature of the firings changes with different values of s with l. For an example, at $I = 0.18$, the sequence of MMOs looks like $1^{10}1^{10}\ldots$ for a long time integration ($t = 100000$) and other forms also possible with different numbers of SAOs with variations in the amplitude of small oscillations (see Fig. 3(d)). At $I = 0.13371$, there exists a supercritical Hopf bifurcation of system (1). There induces canard explosion around the bifurcation point and the system enters into the firing regime. We numerically observe a canard explosion at $I = 0.1488$, where a large amplitude relaxation cycle is observed with variation of a parameter from small amplitude oscillations.

The system also shows an interesting oscillations i.e., MMBOs that are periodic or aperiodic solutions consisting of two different phases. SAOs and LAOs occur alternatively with bursts or multiple large spikes in the LAOs. More than single number of SAOs exhibits in the sequences of SAOs (ranging from one to finitely many). We use the dynamical theory of folded node for the slow–fast system on the number of small amplitude oscillations in the MMOs, that may be controlled by the predominant parameter I. At $I = 0.18$, the DRS system (11) includes $(-0.985277, -0.0147234)$ and $(-0.5 + 0.375269i, -0.5 - 0.375269i)$ as eigenvalues for the equilibrium points ($v^* = -1$, $y^* = 0.111667$) and ($v^* = 1$, $y^* = 1.27833$) respectively. One can easily identify that the first eigenvalue is a folded node and the second is a folded focus. For the folded node, we obtain from the Remark 1(a), $\psi = \frac{|\xi_w|}{|\xi_s|} = \frac{|-0.0147234|}{|-0.985277|} = 0.014943 < 1$ and $\psi^{-1} = 66.9568 \notin \mathbb{N}$. Moreover, $\psi^{-1} = 66.9568$ represents that the weak eigendirection is 66.9568 times weaker than the strong eigendirection. Here, both the strong and weak canard perturb to maximal canard and denoted as primary canards (γ_s and γ_w respectively). We also obtain $n = 32$ satisfying the inequality $2n + 1 < \psi^{-1} < 2n + 3$ and $\psi^{-1} \neq (2n + 2)$. Then in addition to the primary canards $\gamma_{s,w}$, there exists at most 32 other maximal canards, which is known as secondary canards. Thus, there are maximum 34 small amplitude oscillations exhibiting near the folded node. We obtain 10 small amplitude oscillations from numerical simulation which is in good agreement with the analytical results (see Fig. 3(d)). The prediction of exact number of small amplitude oscillations is valid for sufficiently small δ. The exact MMOs pattern can be predicted if $\psi \gg \sqrt{\delta}$ holds [26]. From Remark 1(b), we find that there is no maximal canards exist for the folded focus. Further increasing the external stimulus reduces the number of SAOs in the MMOs. At $I = 0.21$, we found MMOs of type $1^6 1^6 \ldots$ and an interesting phenomenon is observed when we shift the predominant parameter from $I = 0.21$ to $I = 0.225$. Now, the system exhibits MMOs of type $1^4 1^5 1^4 1^5 \ldots$ (see Fig. 3(e)–(f)). Next, the sequence changes to $1^3 1^4 1^3 1^4 \ldots$, $1^3 1^3 \ldots$, $1^2 1^3 1^2 1^3 \ldots$ and $1^2 1^2 \ldots$

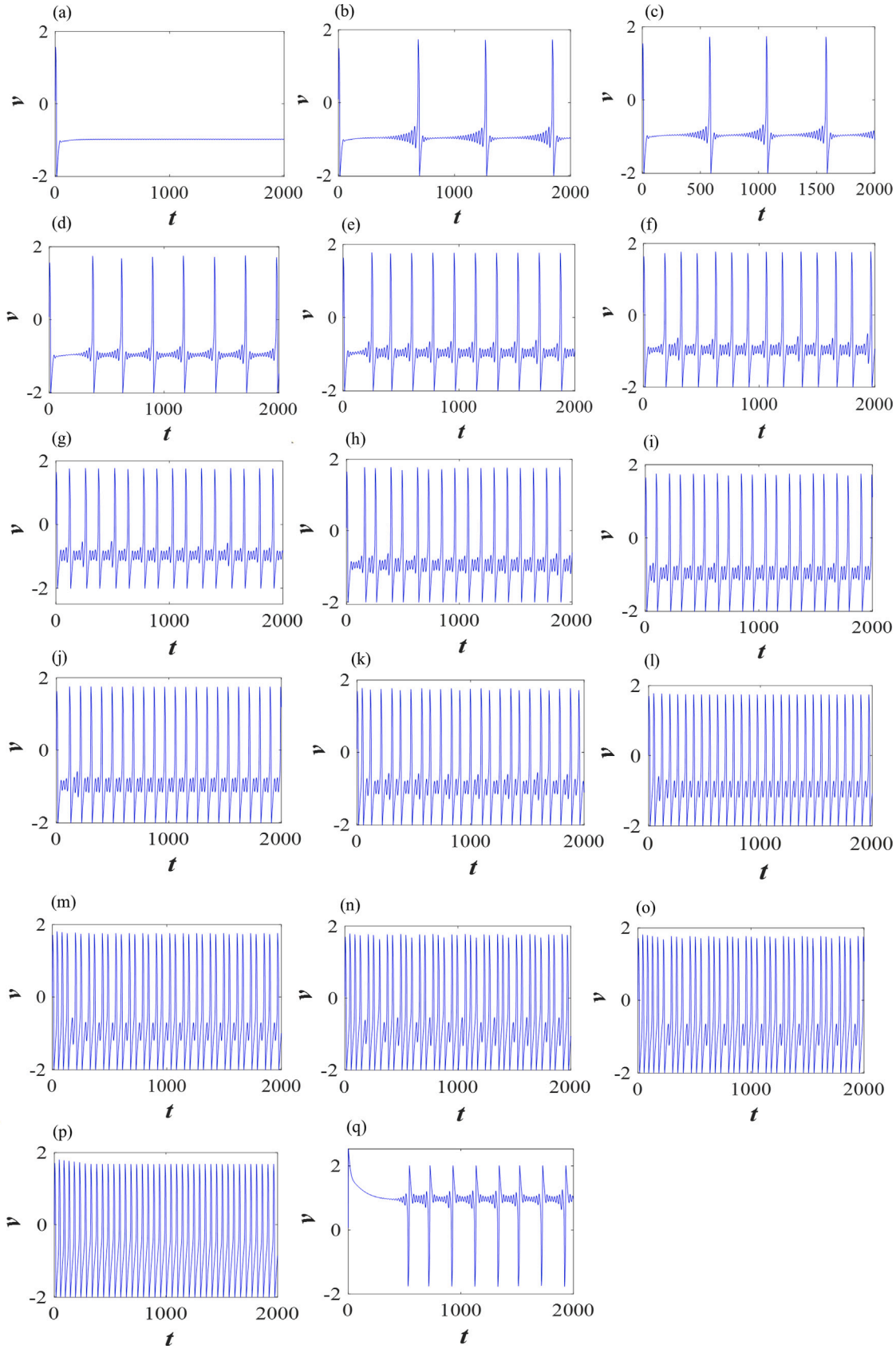

Fig. 3. Various firing responses and transitions of the FHR model with fixed base parameters and the predominant parameter is considered as: (a) $I = 0.0.1$, (b) $I = 0.15$, (c) $I = 0.155$, (d) $I = 0.18$, (e) $I = 0.21$, (f) $I = 0.225$, (g) $I = 0.24$, (h) $I = 0.25$, (i) $I = 0.26$, (j) $I = 0.275$, (k) $I = 0.29$, (l) $I = 0.32$, (m) $I = 0.36$, (n) $I = 0.375$, (o) $I = 0.38$, (p) $I = 0.394$ and (q) $I = 3.1$.

Table 1
The variations of the MMOs patterns with the predominant parameter, I for two different values of δ.

I	0.15	0.155	0.18	0.21	0.225	0.24	0.26	0.29	0.36	0.375	0.38
$\delta = 0.08$	1^{24}	1^{20}	1^{10}	1^{6}	$1^{4}1^{5}$	$1^{3}1^{4}$	$1^{2}1^{3}$	$1^{1}1^{2}1^{2}$	2^{1}	$2^{1}3^{1}$	3^{1}
$\delta = 0.05$	1^{15}	1^{13}	1^{8}	1^{5}	1^{4}	$1^{4}1^{3}1^{3}$	$1^{2}1^{3}$	$1^{1}1^{1}1^{2}$	2^{1}	$2^{1}2^{1}3^{1}$	3^{1}

for $I = 0.24, 0.25, 0.26$ and 0.275 respectively (see Fig. 3(g)–(j)). Again at $I = 0.29$, the pattern of oscillations change to $1^{1}1^{2}1^{2}1^{1}1^{2}1^{2}$... and then it becomes $1^{1}1^{1}$... at $I = 0.32$ (see Fig. 3(k)- (l)). Now, we present the two phases of oscillations, it consists of multiple number of SAOs followed by a doublet, i.e., two large spikes in a single burst, and this pattern repeats again around $I = 0.36$ for a long time range ($t = 100000$). The sequence is $2^{1}2^{1}$... where $l = 2$ and $s = 1$ respectively (Fig. 3(m)). Next, the number of LAOs (l) increases as we increase $I = 0.375$. The sequence follows $2^{1}3^{1}2^{1}3^{1}$... with $l = 2, 3$ and $s = 1$, it generates alternatively (Fig. 3(n)). The number of l again increases and we observe MMBOs with signature $3^{1}3^{1}$... in the similar way at $I = 0.38$ (Fig. 3(o)). SAOs occur around the fold point $v^* = -1$ for all the above cases which we can observe from the time series of the model (see Fig. 3(b)–(o)) and the critical manifold (see Fig. 1(b)).

The transition of firings appears in the system around $I = 0.394$ (i.e., tonic spiking) with stable limit cycle (Fig. 3(p)). The tonic spiking changes to fast spiking behavior at the intermediate phases that again transform into MMOs of another kind. It involves the sequences of one LAOs with one or multiple numbers of SAOs (such as $1^{1}1^{2}1^{1}1^{2}$...), when we further increase the value of $I > 3$, the sequence becomes $1^{7}1^{7}$... around $I = 3.1$ (Fig. 3(q)). Now, the DRS system (11) has folded node for $v^* = 1$, $y^* = -1.64167$ and folded focus $v^* = -1$, $y^* = -2.80833$. The SAOs are generated around the folded node, $v^* = 1$ (see Fig. 3(q)). Again we obtain $\psi = \frac{|\xi_w|}{|\xi_s|} = \frac{|-0.0173683|}{|-0.982632|} = 0.0176753 < 1$ and $\psi^{-1} = 56.5761 \notin \mathbb{N}$ (from Remark 1(a)). Here, the strong eigendirection is 56.5761 times stronger than the weak eigendirection. The inequality holds in good agreement for $n = 27$, i.e., there are at most 27 secondary canards in addition to the primary canards. Thus, there exists maximum 29 SAOs around the fold point. Fig. 3(q) suggests that the system generates only 7 SAOs, which is in the limit of the prediction. Next, with further increase of I, it goes to the quiescent regime. We show the variations in the firing patterns for two different values of small time scale parameter, δ as we change the input current stimulus, I (see 1).

The sequences of MMOs appear in the intermediate periodic to chaotic states that can be observed in the bifurcation diagram. The MMOs can be observed as the alternating periodic states to Farey sequences. The transition phases of MMOs via Farey sequence are observed. Apart from primary and secondary MMOs, the FHR system exhibits unique sequence of periodic MMOs as we vary the predominant parameter (I). These unique sequence of periodic MMOs is known as Farey sequence [48] i.e., it appears like $1^{0} \to \infty^{1} \to l^{1} \to 1^{s} \to 1^{\infty}$, when the control parameter moves slowly to homoclinity. 1^{0} indicates the large amplitude limit cycles in the phase space with tonic spiking, while ∞^{1} denotes a long term tonic spiking or periodic oscillations with the transition to a small amplitude oscillation for once in the complete oscillatory domain. Then it switches to regular or irregular MMOs and MMBOs with different numbers of l and s. The signature of homoclinic chaos is 1^{∞}, where one large amplitude oscillation occurs with countably many irregular small amplitude oscillations. The Farey sequence observed here is $1^{m} \to ...1^{10}... \to ...1^{6}... \to ...1^{4}1^{5}... \to 1^{3}1^{4} \to ...1^{0} \to ...1^{7}$ (see Fig. 3(b, d-g and p-q)).

Now, we explore the homoclinic chaos in the system (1) and try to find out the chaotic windows in the system. The condition for homoclinic chaos holds for $I \in [0.134, 0.159]$ and $[3.142, 3.166]$ with fixed value of $c = -0.775$. At $I = 0.15$, the unique real equilibrium point is obtained as ($v^* = -0.962341$, $w^* = -0.327926$, $y^* = 0.187341$). The discriminant, D of $P(\eta)$ is evaluated at the above mentioned fixed point as $D = -0.00219987 < 0$. The negative value of D indicates that $P(\eta)$ has one real root and a pair of complex conjugate roots as $(-0.0109013, 0.00720096 \pm 0.285853i)$. The conditions of homoclinic chaos hold, i.e., $\sigma = -0.0109013 < 0, \eta_1 = 0.00720096 > 0$ and $|\frac{\sigma}{\eta_1}| = |\frac{-0.0109013}{0.00720096}| = 1.51386 > 1$. Saddle value and saddle index are obtained as $\sigma_1 = -0.00370034$ and $\nu = 0.6605597$ respectively. Here, we obtain $\sigma_1 < 0$ and $\nu < 1$, which indicates that the system (1) has simple dynamics near the saddle focus. The phase portraits with corresponding time series of FHR model in the homoclinic chaos regime are shown in Fig. 4(a-d) for different I. We observe the spiraling trajectories around the saddle focus in all the phase portraits. We also evaluate the Lyapunov exponents (LEs) as a function of time and the predominant parameter I to show the chaotic behavior of the system (1). First, we consider the LEs as a function of time and we plot the spectrum for $I = 0.15$. We found the Lyapunov coefficients as $(0.000079, -0.000054 - 0.053439)$. The positive first Lyapunov coefficient (see Fig. 4(e), red curve) indicates that the system exhibits chaos. Fig. 4(f) depicts the LEs spectrum in the interval $I \in [0.134, 0.159]$ and it is found that the first LE is positive in this interval. Therefore, the system is chaotic in this interval. The system (1) exhibits MMOs with one large and finitely many irregular small amplitude oscillations (1^{∞}) in this interval (see Fig. 3(b) and (c)). Thus, we observe MMOs as a transition route to homoclinic chaos. Again at $I = 3.1440$, the real equilibrium point is obtained as ($v^* = 0.962341$, $w^* = 2.07793$, $y^* = -1.73734$). Similar to the above case, we found that $D = -0.00219987 < 0$. The corresponding eigenvalues of the system are obtained as $(-0.0109168, 0.00986154 \pm 0.285222i)$ and the conditions of homoclinic chaos hold, i.e., $\sigma = -0.0109168 < 0, \eta_1 = 0.00986154 > 0$ and $|\frac{\sigma}{\eta_1}| = |\frac{-0.0109168}{0.00986154}| = 1.107 > 1$. Again, the system has simple dynamics near the saddle focus as $\sigma_1 < 0$ and $\nu < 1$. The LEs spectrum with respect to I is plotted for $I \in [3.142, 3.166]$ and we found that the first LE is positive in this interval, which indicates that the system (1) exhibits chaos in this interval (see Fig. 4(g)).

6. Conclusions

This study is concerned with the MMOs and MMBOs in the slow–fast FHR model, where the dynamics evolves on multiple time scales and its bifurcation structure. We have considered the dynamics of the FHR model with the predominant bifurcation parameter, I and study different regions of firing characteristics. We prove the validation of the existence of Hopf bifurcations and canard phenomenon. We illustrate the parameter space of canard phenomenon where MMOs occur and our numerical simulations involved the solution of the dynamical system of ODEs. Further, we justify the existence of maximum number of SAOs between two consecutive LAOs via folded node theory. The slow dynamics of model is explored using the reduced system (8) and corresponding critical manifold in two and three dimensions. Interestingly, we can categorize the generations of MMOs and MMBOs into two different classes. One in which the SAOs are generated near the point L^- and in another class the SAOs are generated near the point L^+ (see Fig. 3).

The threshold of MMOs and chaotic behavior have been studied numerically. MMBOs consisting of SAOs and LAOs with fast oscillations of bursts that add spikes adding transition. At the boundaries of it, there exists different dynamical regimes such as MMOs, quiescence, tonic spiking etc. General results have been derived for a finite dimensional slow–fast systems with the emergence of MMOs, that could be applied in this direction and heterogeneous system parameters may be introduced for further investigation. Moreover, this type of phenomenological biophysical model provides us a theoretical framework to analyze the dynamical characteristics of healthy and diseased neurons that can be found in experimental results [40]. Previously, MMBOs were observed as the dynamical behavior of the GnRH model neuron in a small-size network, which can be helpful in the studies for

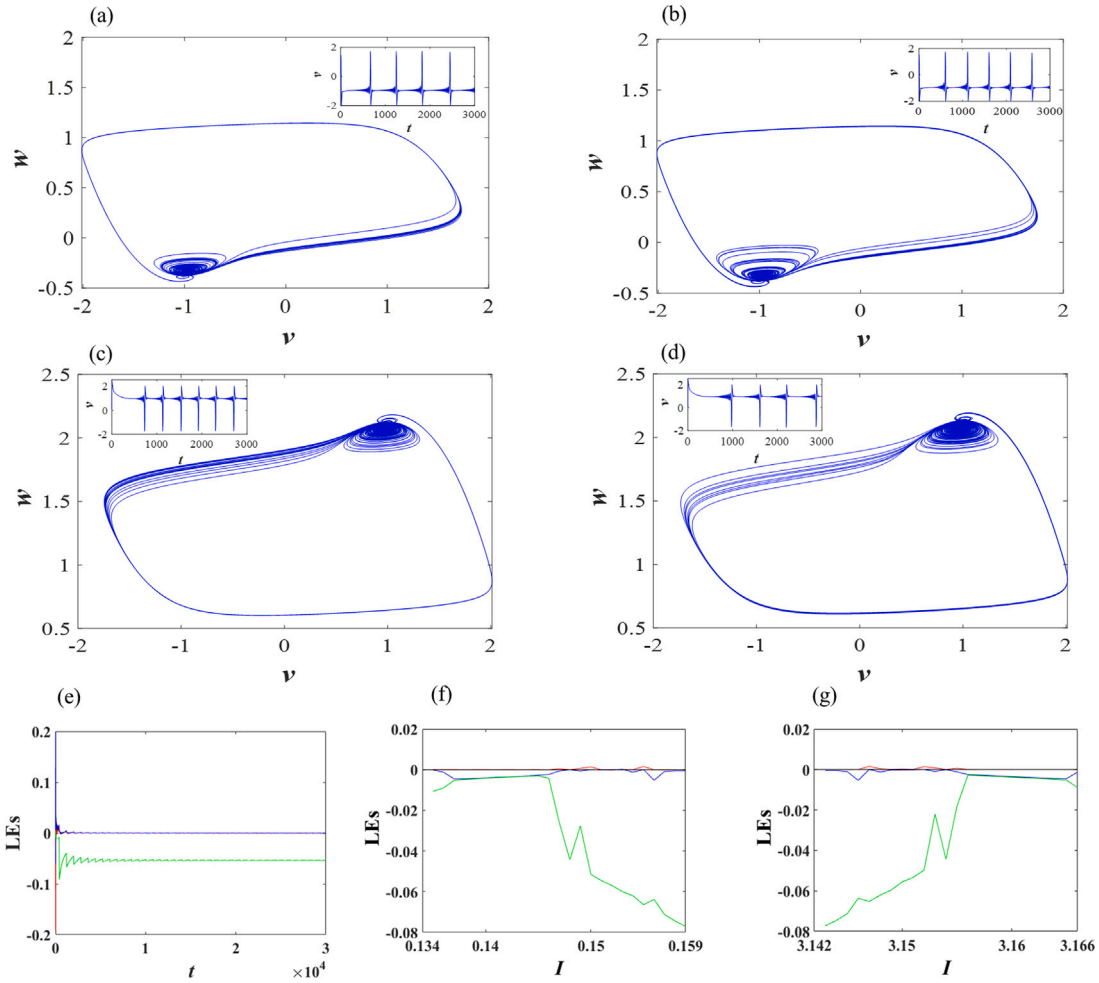

Fig. 4. Phase portraits and corresponding time series of FHR model in the homoclinic chaos slow–fasts for (a) $I = 0.15$, (b) $I = 0.155$, (c) $I = 3.142$ and (d) $I = 3.155$. Dynamics of Lyapunov spectrum of the model: (e) LEs as a function of time for $I = 0.15$, (f)–(g) LEs as a function of I in the intervals $I \in [0.134, 0.159]$ and $I \in [3.142, 3.166]$ respectively. (For interpretation of the references to color in this figure legend, the reader is referred to the web version of this article.)

epilepsy [21]. MMBOs are a combination of time series of canard mediated MMOs and bursting oscillations. In complex biophysical systems, different mechanisms play during the oscillatory phases that produce spike patterns between fast and slow amplitude motions, known as MMOs. The pyramidal neurons can generate two different types of MMOs and the characterization of these MMOs was inspected under antiepileptic drug conditions [43,58]. MMOs can be observed in various types of neurons such as in the neocortex neurons, hippocampal CA1 neurons, thalamus, spinal motor neurons etc. [41,59].

The transition from the peak of the action potential to steady states can be achieved by reducing neuronal gain with the help of MMOs [41,50]. The impacts of SAOs or subthreshold oscillations on different neuronal responses were studied in [59,60]. In the evolution of MMOs and controlling spike clustering, the SAOs play an interesting role [61,62]. Further, SAOs effect on the sensitivity of neurons with the variations in synaptic inputs and network synchronization for certain firing frequencies [13]. We discussed a number of possible biophysical interpretations on the roles of MMOs and it may be useful for the researchers working in mathematical modeling and dynamical systems that play a crucial role in understanding neuronal rhythmic behavior. Such mixed mode oscillations (MMOs and MMBOs) are of great interest in current research, and it includes experimental, theoretical and computational approaches in biological systems. Further, this type of work may be extended from coupled systems to biophysical systems with different network structures so as to investigate possible applications in this direction.

CRediT authorship contribution statement

Sanjeev Kumar Sharma: Conceptualization, Worked on the analytical and numerical results, Writing – original draft. **Arnab Mondal:** Worked on the analytical and numerical results. **Argha Mondal:** Designed the work, Worked on analytical and numerical results, Writing – original draft. **M.A. Aziz-Alaoui:** Reviewing and editing the manuscript with constructive suggestions. **Ranjit Kumar Upadhyay:** Reviewing and editing the manuscript with constructive suggestions. **Jun Ma:** Reviewing and editing the manuscript with constructive suggestions.

Declaration of competing interest

The authors declare that they have no known competing financial interests or personal relationships that could have appeared to influence the work reported in this paper.

Data availability

No data was used for the research described in the article.

Acknowledgments

This work is supported by the National Board for Higher Mathematics (NBHM), India, Department of Atomic Energy, Govt. of India under Grant No. 02011/11/2022NBHM(R.P)/R & D-II/10217 to the author Argha Mondal.

References

[1] Rinzel J, Troy WC. Bursting phenomena in a simplified oregonator flow system model. J Chem Phys 1982;76(4):1775–89.
[2] Rinzel J. A formal classification of bursting mechanisms in excitable systems. In: Mathematical topics in population biology, morphogenesis and neurosciences. Springer; 1987, p. 267–81.
[3] Izhikevich EM. Synchronization of elliptic bursters. SIAM Rev 2001;43(2):315–44.
[4] Wojcik J, Shilnikov A. Voltage interval mappings for an elliptic bursting model. In: Nonlinear dynamics new directions. Springer; 2015, p. 195–213.
[5] Izhikevich EM. Neural excitability, spiking and bursting. Int J Bifurcation Chaos 2000;10(06):1171–266.
[6] Rinzel J, Huguet G. Nonlinear dynamics of neuronal excitability, oscillations, and coincidence detection. Comm Pure Appl Math 2013;66(9):1464–94.
[7] Izhikevich EM. Simple model of spiking neurons. IEEE Trans Neural Netw 2003;14(6):1569–72.
[8] Ma J, Tang J. A review for dynamics in neuron and neuronal network. Nonlinear Dynam 2017;89(3):1569–78.
[9] Coombes S, Bressloff PC. Bursting: The genesis of rhythm in the nervous system. World Scientific; 2005.
[10] Brø ns M, Bar-Eli K. Canard explosion and excitation in a model of the Belousov-Zhabotinskii reaction. J Phys Chem 1991;95(22):8706–13.
[11] Brøns M, Kaper TJ, Rotstein HG. Introduction to focus issue: Mixed mode oscillations: Experiment, computation, and analysis. 2008.
[12] Desroches M, Guckenheimer J, Krauskopf B, Kuehn C, Osinga HM, Wechselberger M. Mixed-mode oscillations with multiple time scales. Siam Rev. 2012;54(2):211–88.
[13] Bacak BJ, Kim T, Smith JC, Rubin JE, Rybak IA. Mixed-mode oscillations and population bursting in the pre-Bötzinger complex. Elife 2016;5:e13403.
[14] An X, Qiao S. The hidden, period-adding, mixed-mode oscillations and control in a HR neuron under electromagnetic induction. Chaos Solitons Fractals 2021;143:110587.
[15] Zhang C, Ma X, Bi Q. Complex mixed-mode oscillations based on a modified Rayleigh-duffing oscillator driven by low-frequency excitations. Chaos Solitons Fractals 2022;160:112184.
[16] Szmolyan P, Wechselberger M. Canards in R^3. J Differential Equations 2001;177(2):419–53.
[17] Wechselberger M. Existence and bifurcation of canards in R^3 in the case of a folded node. SIAM J Appl Dyn Syst 2005;4(1):101–39.
[18] Desroches M, Krauskopf B, Osinga HM. The geometry of slow manifolds near a folded node. SIAM J Appl Dyn Syst 2008;7(4):1131–62.
[19] Desroches M, Freire E, Hogan SJ, Ponce E, Thota P. Canards in piecewise-linear systems: explosions and super-explosions. Proc. R. Soc. A 2013;469(2154):20120603.
[20] Kovacic I, Cartmell M, Zukovic M. Mixed-mode dynamics of bistable oscillators with low-frequency excitation: behavioural mapping, approximations for motion and links with van der Pol oscillators. Proc R Soc Lond Ser A Math Phys Eng Sci 2015;471:20150638.
[21] Desroches M, Kaper TJ, Krupa M. Mixed-mode bursting oscillations: Dynamics created by a slow passage through spike-adding canard explosion in a square-wave burster. Chaos 2013;23(4):046106.
[22] Benoit E, et al. Chasse au canard. Collect. Math. 1981;32:37–119.
[23] Guckenheimer J, Kuehn C. Computing slow manifolds of saddle type. SIAM J Appl Dyn Syst 2009;8(3):854–79.
[24] Ambrosio B, Aziz-Alaoui M, Yafia R. Canard phenomenon in a slow-fast modified Leslie–Gower model. Math Biosci 2018;295:48–54.
[25] Drover J, Rubin J, Su J, Ermentrout B. Analysis of a canard mechanism by which excitatory synaptic coupling can synchronize neurons at low firing frequencies. SIAM J Appl Math 2004;65(1):69–92.
[26] Rotstein HG, Wechselberger M, Kopell N. Canard induced mixed-mode oscillations in a medial entorhinal cortex layer II stellate cell model. SIAM J Appl Dyn Syst 2008;7(4):1582–611.
[27] Desroches M, Krauskopf B, Osinga HM. Mixed-mode oscillations and slow manifolds in the self-coupled FitzHugh-Nagumo system. Chaos 2008;18(1):015107.
[28] Nowacki J, Osinga HM, Tsaneva-Atanasova K. Dynamical systems analysis of spike-adding mechanisms in transient bursts. J Math Neurosci 2012;2(1):7.
[29] Rubin J, Wechselberger M. The selection of mixed-mode oscillations in a Hodgkin-Huxley model with multiple timescales. Chaos 2008;18(1):015105.
[30] Muratov CB, Vanden-Eijnden E. Noise-induced mixed-mode oscillations in a relaxation oscillator near the onset of a limit cycle. Chaos 2008;18(1):015111.
[31] Upadhyay RK, Mondal A, Teka WW. Mixed mode oscillations and synchronous activity in noise induced modified Morris–Lecar neural system. Int J Bifurcation Chaos 2017;27(05):1730019.
[32] Kummer U, Olsen LF, Dixon CJ, Green AK, Bornberg-Bauer E, Baier G. Switching from simple to complex oscillations in calcium signaling. Biophys J 2000;79(3):1188–95.
[33] Rotstein HG, Kuske R. Localized and asynchronous patterns via canards in coupled calcium oscillators. Physica D 2006;215(1):46–61.
[34] Liu P, Liu X, Yu P. Mixed-mode oscillations in a three-store calcium dynamics model. Commun Nonlinear Sci Numer Simul 2017;52:148–64.
[35] Krupa M, Popović N, Kopell N, Rotstein HG. Mixed-mode oscillations in a three time-scale model for the dopaminergic neuron. Chaos 2008;18(1):015106.
[36] Davison EN, Aminzare Z, Dey B, Ehrich Leonard N. Mixed mode oscillations and phase locking in coupled FitzHugh-Nagumo model neurons. Chaos 2019;29(3):033105.
[37] Vo T, Bertram R, Tabak J, Wechselberger M. Mixed mode oscillations as a mechanism for pseudo-plateau bursting. J Comput Neurosci 2010;28(3):443–58.
[38] Baldemir H, Avitabile D, Tsaneva-Atanasova K. Pseudo-plateau bursting and mixed-mode oscillations in a model of developing inner hair cells. Commun Nonlinear Sci Numer Simul 2020;80:104979.
[39] Bertram R, Rhoads J, Cimbora WP. A phantom bursting mechanism for episodic bursting. Bull Math Biol 2008;70(7):1979.
[40] Erchova I, McGonigle DJ. Rhythms of the brain: An examination of mixed mode oscillation approaches to the analysis of neurophysiological data. Chaos 2008;18(1):015115.
[41] Iglesias C, Meunier C, Manuel M, Timofeeva Y, Delestrée N, Zytnicki D. Mixed mode oscillations in mouse spinal motoneurons arise from a low excitability state. J Neurosci 2011;31(15):5829–40.
[42] Krupa M, Ambrosio B, Aziz-Alaoui M. Weakly coupled two-slow–two-fast systems, folded singularities and mixed mode oscillations. Nonlinearity 2014;27(7):1555.
[43] Ghosh S, Mondal A, Ji P, Mishra A, Dana SK, Antonopoulos CG, Hens C. Emergence of mixed mode oscillations in random networks of diverse excitable neurons: the role of neighbors and electrical coupling. Front. Comput. Neurosci. 2020;14(49):1–11.
[44] Izhikevich EM. Which model to use for cortical spiking neurons? IEEE Trans Neural Netw 2004;15(5):1063–70.
[45] Del Negro CA, Hsiao C-F, Chandler SH, Garfinkel A. Evidence for a novel bursting mechanism in rodent trigeminal neurons. Biophys J 1998;75(1):174–82.
[46] Belykh V, Pankratova E. Chaotic synchronization in ensembles of coupled neurons modeled by the FitzHugh-Rinzel system. Radiophys. Quantum Electron. 2006;49(11):910–21.
[47] Xie W, Xu J, Cai L, Jin Y. Dynamics and geometric desingularization of the multiple time scale Fitzhugh Nagumo Rinzel model with fold singularity. Commun Nonlinear Sci Numer Simul 2018;63:322–38.
[48] Chakraborty S, Dana SK. Shil'nikov chaos and mixed-mode oscillation in Chua circuit. Chaos 2010;20(2):023107.
[49] Shilnikov LP, Shilnikov A. Shilnikov bifurcation. Scholarpedia 2007;2(8):1891.
[50] Golomb D. Mechanism and function of mixed-mode oscillations in vibrissa motoneurons. PLoS One 2014;9(10).
[51] Krupa M, Popović N, Kopell N. Mixed-mode oscillations in three time-scale systems: a prototypical example. SIAM J Appl Dyn Syst 2008;7(2):361–420.
[52] De Maesschalck P, Kutafina E, Popović N. Three time-scales in an extended Bonhoeffer–van der Pol oscillator. J Dynam Differential Equations 2014;26(4):955–87.
[53] Ambrosio B, Françoise J-P. Propagation of bursting oscillations. Phil Trans R Soc A 2009;367(1908):4863–75.
[54] Brø ns M, Krupa M, Wechselberger M. Mixed mode oscillations due to the generalized canard phenomenon. Fields Inst. Commun. 2006;49:39–63.
[55] Wechselberger M. A propos de canards (apropos canards). Trans Amer Math Soc 2012;364(6):3289–309.
[56] Guckenheimer J, Lizarraga I. Shilnikov homoclinic bifurcation of mixed-mode oscillations. SIAM J Appl Dyn Syst 2015;14(2):764–86.
[57] Dhooge A, Govaerts W, Kuznetsov YA. MATCONT: a MATLAB package for numerical bifurcation analysis of ODEs. ACM Trans Math Softw 2003;29(2):141–64.
[58] Babak V, Ghaffari MK, Sherif ME. Mixed-mode oscillations in pyramidal neurons under antiepileptic drug conditions. PLoS One 2017;12(6).
[59] Narayanan R, Johnston D. Long-term potentiation in rat hippocampal neurons is accompanied by spatially widespread changes in intrinsic oscillatory dynamics and excitability. Neuron 2007;56(6):1061–75.
[60] Engel TA, Schimansky-Geier L, Herz AV, Schreiber S, Erchova I. Subthreshold membrane-potential resonances shape spike-train patterns in the entorhinal cortex. J Neurophysiol 2008;100(3):1576–89.
[61] Torben-Nielsen B, Segev I, Yarom Y. The generation of phase differences and frequency changes in a network model of inferior olive subthreshold oscillations. PLoS Comput Biol 2012;8(7).
[62] Latorre R, Torres JJ, Varona P. Interplay between subthreshold oscillations and depressing synapses in single neurons. PLoS One 2016;11(1).